ATMOSPHERIC SCIENCE LETTERS
Atmos. Sci. Let. (2015)
Published online in Wiley Online Library
(wileyonlinelibrary.com) **DOI:** 10.1002/asl2.558

RMetS
Royal Meteorological Society

Does convection vary in different cloud disturbances?

Yoshiaki Miyamoto,[1]* Ryuji Yoshida,[1] Tsuyoshi Yamaura,[1] Hisashi Yashiro,[1] Hirofumi Tomita[1,2] and Yoshiyuki Kajikawa[1]

[1]*RIKEN Advanced Institute for Computational Science, Kobe, Japan*
[2]*Seamless Environmental Prediction Research, Japan Agency for Marine-Earth Science and Technology, Yokohama-city, Kanagawa, Japan*

**Correspondence to:*
Y. Miyamoto, RIKEN Advanced Institute for Computational Science, 7-1-26, Minatojima-minami-machi, Chuo-ku, Kobe, Hyogo 650-0047, Japan.
E-mail: ymiyamoto@riken.jp

Received: 18 June 2014
Revised: 14 December 2014
Accepted: 17 December 2014

Abstract

Deep moist convection is an element of cloud disturbances such as Madden-Julian oscillation (MJO), tropical cyclones (TCs), mid-latitudinal low depressions (MDL), and fronts (FRT). However, differences in convection characteristics in disturbances remain unclear. We first clarified the statistical features of the convection (structure, intensity, and environmental parameters) in various disturbances simulated by a global simulation with a sub-kilometre grid spacing. The convection in MJO (TC) was tall with a strong (weak) upward motion, and was driven by large convective available potential energy (strong low-level convergence). The convection in MDL and FRT was shorter and characterized by a strong vertical wind shear.

Keywords: **global simulation; moist convection; cloudy disturbance**

1. Introduction

Cloud systems on Earth are globally distributed, varying from individual cloud cells (10^0 km) to large-scale cloud disturbances (10^4 km). The cloud disturbances play important roles in modifying the global-scale energy budget. Additionally, the disturbances often accompany heavy rainfall and hence cause severe disasters around the world. Consequently, researchers have paid special attention to understanding their physical processes. It is widely recognized that these disturbances are driven by interaction with deep moist convection; a number of convection cells are produced under strong forcing of the disturbances. In turn, the convection itself affects its background (i.e. the disturbances) by transporting mass, momentum, and thermal energy. For instance, the intensity and structure of TCs are significantly sensitive to convective activities in the core region (e.g. Smith, 2000). Hence, for a better understanding of disturbances, their interaction with convection needs to be examined.

There is great difficulty in studying the interaction between the convection and disturbances due to the large-scale gap in both temporal and spatial dimensions. Convection has temporal and spatial scales from 30 min to 1 h and from less than 1–10 km (Houze, 1994), whereas disturbance timescales are 1 week to 1 month and 10^2–10^4 km (Madden and Julian, 1994). Detailed datasets ranging from individual convective cells to entire disturbances are hard to obtain, especially from observations and even from numerical simulations due to computer resource limitations. Hence, previous studies have numerically examined the interaction by parameterizing the convection and/or limiting the target field covering a particular disturbance. Because convection parameterizations can represent the *effects* of convection on the disturbances, only responses of the disturbances to energy transport by the convection have been understood previously.

However, the understanding of convection structures and intensities in the disturbances has remained limited. Convection features such as the maximum vertical velocity appear to be different from one disturbance to another. Convection largely depends on its environment, and the structures and/or driving mechanisms of the disturbances mentioned above are different in each disturbance. For a better understanding of the disturbances, an understanding of differences in convection features is highly desirable.

Here, we elucidate differences in convection structures and intensity in cloud disturbances based on the results of a sub-kilometre global simulation. Section 2 describes the simulation data and the methodology to detect convection and disturbances. Results and discussion are presented in Section 3. Section 4 provides the concluding remarks.

2. Simulation data and definition of cloud disturbances

We used simulation results with 0.87-km grid spacing (Miyamoto *et al.*, 2013) without convection parameterization, which had been performed using nonhydrostatic icosahedral atmospheric model (NICAM) (Tomita and Satoh, 2004; Satoh *et al.*, 2008) on the K computer. They showed that the simulation realistically captures the global cloud field and convective cells. This dataset enabled us to compare convection generated in disturbances under realistic conditions. To detect both convective cells and disturbances, simple methodologies developed previously (Miyamoto *et al.*, 2013) were

applied to the simulated results. These were used uniformly across a global dataset.

The number of vertical model layers was 94, which was vertically stretched. The height of the lowest level was 36 m, and the average grid spacing in the troposphere was about 250 m. Physical processes such as solar radiation and boundary-layer turbulence were solved using parameterizations (Louis, 1979; Nakanishi and Niino, 2004; Tomita, 2008; Sekiguchi and Nakajima, 2009; Noda *et al.*, 2010). The initial conditions in the simulation were constructed using the results of a 3-day integration at 3.5-km grid spacing in which the initial conditions were obtained from linearly interpolated data from the final analysis of the National Centre for Atmospheric Research (Kalnay *et al.*, 1996). The simulation period was 12 h.

The convection was detected from the simulated results by the following two-step method (Miyamoto *et al.*, 2013). First, convective grids were defined by the optical thickness (>35) and cloud-top pressure (<400 hPa) following the cloud separation scheme of the International Satellite Cloud Climatology Project (ISCCP; Rossow and Schiffer, 1999). Then, the convection core was detected in the convective grids as the grid at which the vertically averaged vertical velocity in the troposphere was greater than that in all neighbouring grids.

As large-scale atmospheric cloud disturbances, four disturbances were chosen in the present study: the Madden-Julian oscillations (MJO), tropical cyclones (TCs), mid-latitudinal low-pressure disturbances (MDL), and synoptic-scale fronts (FRT). To extract the MJO signal in the outgoing longwave radiation (OLR) from the NOAA satellite (Liebmann and Smith, 1996), the boreal summer intraseasonal oscillation index (Kikuchi *et al.*, 2012) was applied. The MJO region was defined as the grid where the filtered OLR was less than $-10\,\mathrm{W\,m^{-2}}$. The TCs were extracted by Miyamoto *et al.*'s (2014) methodology. The TC region was defined as that inside the 600-km radius from the centre. To detect the MDL centres, the simulated data were coarsened to $2.5 \times 2.5^\circ$ grid spacing. Then, grids at which the sea-surface pressure (SLP) was 5 hPa less than the areal average in the 10° radius were detected as low centres. The MDL region was assumed to be 1000 km from the low-pressure minimum. The frontal region was detected by the thermal frontal locator (Renard and Clarke, 1965), which represented a third-order differential of a variable in the horizontal direction with a direction modulation term. The equivalent potential temperature at the 1500-m level was employed as the variable in the thermal frontal locator. The grids where the thermal frontal locator was $>10^{-13}$ in the $2.5 \times 2.5^\circ$ data were first detected. Then, if the girds had a continuous region whose maximum distance was greater than 10°, the region was detected as frontal grids. The frontal regions were defined as those inside the 200-km distance from the frontal grids.

3. Results and discussion

Figure 1(a) shows the simulated cloud field at 201208251200UTC in the sub-kilometre simulation with the detected convection centre grids and disturbances. The simulation successfully reproduced multi-scale cloudy convective phenomena ranging from 10° to 10^4 km in a single simulation. The disturbance regions (MJO, red; TC, blue; MDL, green; and FRT, cyan) were reasonably detected. The MJO region was detected at 90°–120° longitude and −15° to 15° latitude. Although re-analysis data were used to detect the MJO, simulated organized convective systems were seen in the MJO region. Two TCs were extracted at (lon, lat) = (123.5, 17.52) and (128.5, 25.90). The best track data of the Joint Typhoon Warning Centre showed that there were actually two TCs around these points at this time. Further analysis showed that the TCs are in the quasi-steady stage. Especially the TC close to Japan has developed well, and has a clear eye. MJO is a large scale (a few thousand km) envelop of convection with circulation, whereas TC is a relatively small scale (a few hundred km) convective phenomenon. Since the TCs are distant from the MJO region, it is strongly suggested that the TCs are not related to the MJO. In the mid-latitudes, both MDL and FRT regions were widely detected, especially in the regions of low OLR. Thus, compared with the cloud field, the locations of each disturbance were reasonable. Convection cores were also detected reasonably frequently in low-OLR regions (e.g. low-latitude regions in the western Pacific or mid-latitude cyclonic regions), as found previously (Miyamoto *et al.*, 2013). Figure 1(b) displays the latitudinal distributions and the number of convective cells in the different disturbances. The convection associated with the MJO exists around the equatorial region, that associated with TCs is detected only in the northern hemisphere, and those of MDL and FRT are distributed mainly in latitudes ±30° to ±60°. The spatial distributions of convection and disturbances are reasonable at all latitudes.

Figure 2 shows the radius-height cross-sections for the vertical velocity w composed of all convection in each disturbance, as well as the global average. The convection structure and intensity are significantly different in each disturbance. The convection in the MJO has the strongest w value among the four disturbances and global average. It is also stronger than the average at the same latitudes (not shown). The MJO convection accompanies the strongest precipitation, and the peak is located at the core and decays with radius. The strong precipitation is consistent with the strong upward motion and with the large downdraft at the bottom of atmosphere. The convection in the TC has a tall structure similar to that in the MJO, but w is weaker. It is even weaker than the average at the corresponding latitudes. Unlike the MJO convection, w at the bottom is not generally negative, but slightly positive. Consistent with these parameters, the precipitation is smaller than that of the MJO. In the mid-latitudinal disturbances (i.e.

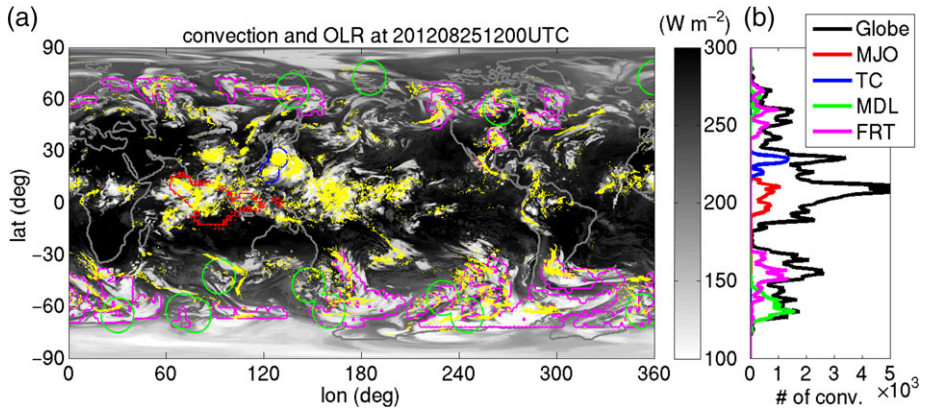

Figure 1. (a) Horizontal distribution of the extracted convection core in Δ0.87 (yellow) superimposed on the OLR (shaded) at 201208251200UTC. The regions enclosed by the red, blue, green, and magenta contours indicate regions detected as the MJO, TC, MDL, and FRT disturbances, respectively. (b) Latitudinal profile of the number of extracted convective cells in the four classes of disturbances in a 1° latitude bin.

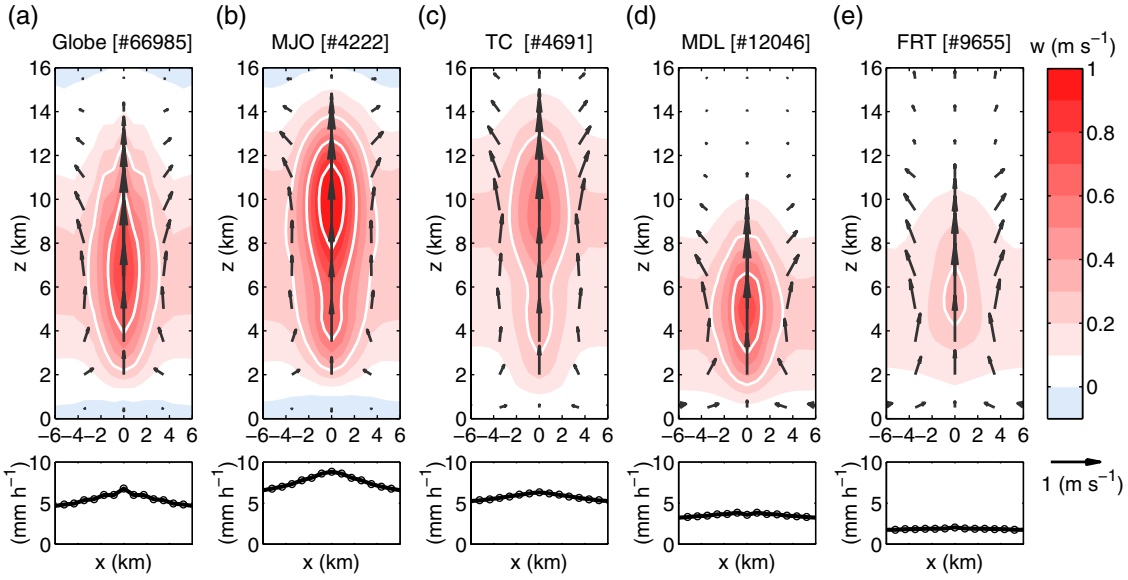

Figure 2. (Top) Radius-height cross-sections for composites of vertical velocity w (shaded) and velocity vector of radial velocity and w (arrows) for the simulated convection detected in (a) the globe, (b) MJO, (c) TC, (d) MDL, and (e) FRT. The contours at $w = 0.3$, 0.6, and 0.9 m s^{-1} are highlighted by the white lines. The number of convection cells is shown in the figure title. (Bottom) Radial distributions of precipitation averaged from all detected convection.

MDL and FRT), the convection is shorter than those in the two tropical disturbances; the peak height of w is located around 5–6 km. The convection in the MDL has stronger w than that in the FRT, or even in the TC. The precipitation is accordingly stronger in the MDL than in the FRT. However, compared with the tropical disturbances, the amount of precipitation and radial gradient in the MDL and FRT convection are small. In short, the convection structure largely depends on the disturbances: the convection in tropical disturbances has stronger maximum w at a higher level compared with that in the mid-latitudinal disturbances, and the amount of precipitation is correspondingly large in the tropical disturbances.

To explore the differences in convection environments, Figure 3 shows the convection distance and environmental parameters (i.e. low-level mass convergence, CAPE, and vertical shear of horizontal winds), which are closely related to the physical processes of convection. The environmental parameters are areally averaged inside the 30-km radius from the convection centre. The differences in the medians of all parameters satisfy the 99% level of statistical significance. The distance to the nearest convection centre is shortest in the TC of the four disturbances, with a median of 4.35 km (=5 *model grids*), and 50% of the convection in the TC has a nearest convection centre at 2.61–6.02 km (3–7 grids) distance. In the other disturbances, the median is 5.22 km (6 grids). This indicates that the number density of the convection is large in the TC compared with those in the other disturbances and the global average.

Figure 3(b) shows that the TC convection has the strongest low-level mass convergence, calculated in the lowest 500 m. The convergence averaged across the entire disturbance is slightly positive in all disturbances. The convergence below the MJO convection is

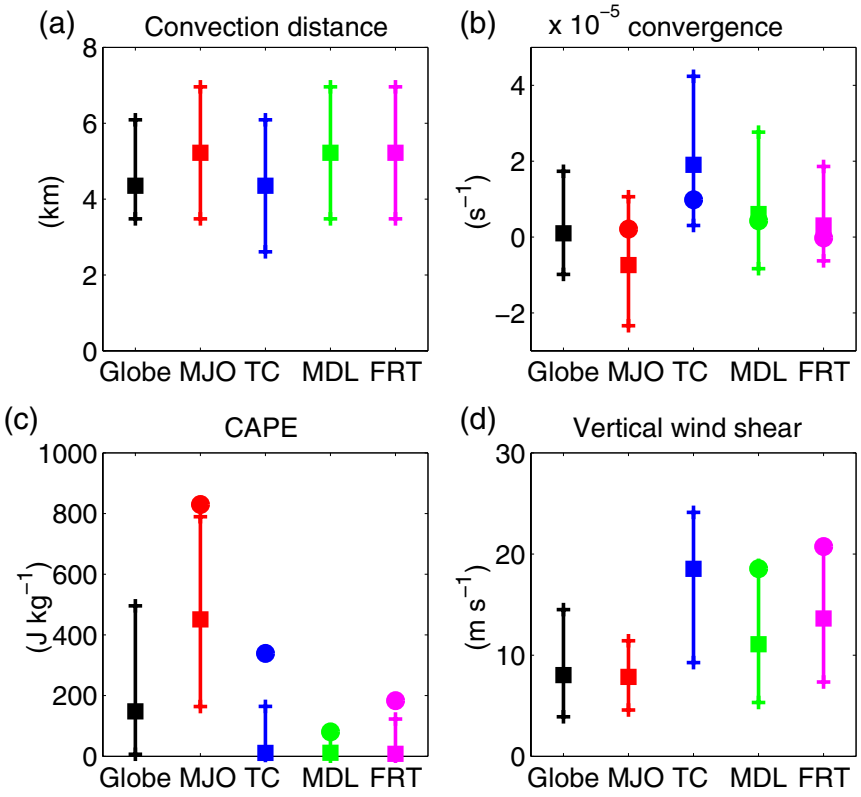

Figure 3. (a) Distance to the nearest convection cell, (b) low-level mass convergence, (c) convection available potential energy (CAPE), and (d) vertical shear of horizontal wind between the 2.5-km height and 2 km below the tropopause. The colours are the same as those in Figure 1. The square and circle indicate the median of the detected convection and the average of all grids diagnosed as disturbances, respectively. The vertical line ranges between the top and bottom quantiles.

negative. This is consistent with the composite presented in Figure 2, which indicates the presence of strong rainfall and horizontal divergence flow. However, the CAPE value is largest in the MJO convection (Figure 3(c)). The averaged CAPE in the entire disturbance and the difference from the disturbance average are most significant in the MJO. This implies that convection in the MJO is driven by consumption of the background CAPE because the convergence in the MJO convection is not strong (Figure 3(b)). The CAPE difference between the convection and disturbance is also large in the TC convection, whereas the difference is quite small in the mid-latitudinal convection. In both the MDL and FRT, the convection is characterized by strong vertical wind shear (that is, the absolute value of the wind-vector difference between the 2.5-km level and 2 km below the tropopause; Figure 3(d)). Specifically, the vertical wind shear is stronger in the FRT convection than in the MDL convection, whereas the convergence is weaker in the MDL.

For more comprehensive understanding of the MJO and TC convection differences based on the different environments, we show the histogram of convection of the globe, and MJO and TC in a CAPE-convergence space (Figure 4). The histograms of MJO and TC convection are the differences from the global convection. It is clearly shown that the MJO (TC) convection tends to have high (low) CAPE and weak (strong) convergence environments compared with the global one. There is another peak for the TC convection in high CAPE and weak convergence range. This is simply because the histogram of global convection tends to have lower CAPE than that of tropical convection, owing to taking account of the mid-latitudinal region whose CAPE is much lower than tropics.

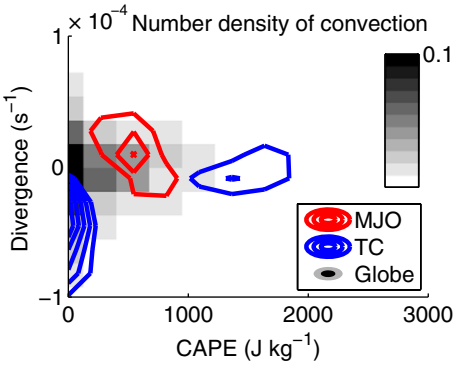

Figure 4. Number distributions of convection in a CAPE-low-level mass convergence space. The numbers are normalized by total number, and are binned into 300 J kg^{-1} and 0.2×10^{-4} intervals. Shaded area shows the global data. The red and blue contours respectively show the differences of convection number in MJO and TC from the global one. Positive values are only plotted. The contour interval is 0.01.

The result indicates that the MJO convection is characterized by strong w and precipitation, high CAPE, and

weak convergence suggests that it is generated by strong thermodynamic forcing. However, the strong convergence, low CAPE, and weak w of the TC convection imply that it is driven by strong background dynamical forcing convergence in relatively low-CAPE environments. The relationship between the maximum vertical velocity and CAPE is consistent with the potentially attainable velocity, $w_{\max} \sim (2\mathrm{CAPE})^{1/2}$. The stronger convergence and relatively weaker vertical wind shear in the MDL convection compared with the FRT are consistent with stronger w in the MDL convection. The convection in the tropical disturbances (MJO and TC) has a tall structure, whereas that in the mid-latitudinal disturbances (MDL and FRT) is short, indicating that convection height is determined by the depth of the troposphere.

4. Concluding remarks

This study elucidated the convection differences in various atmospheric disturbances (MJO, TC, MDL, and FRT). The cloud-top height is clearly different between the tropical disturbances (MJO and TC) and mid-latitudinal ones (MDL and FRT). The MJO convection has a strong upward motion and precipitation, whereas the TC convection has a weak updraft. The MDL convection is characterized by relatively strong convergence and weak vertical wind shear compared with the FRT convection. The differences may be attributable to the environmental fields of the convection (i.e. the disturbances themselves): the MJO (TC) convection is generated under a high (low) CAPE and relatively weak (strong) convergence region. Therefore, the feedback process of convection within the disturbance appears to be significantly different in each disturbance. The present study analysed a snapshot of global simulation result with a high spatial resolution. We emphasize the importance of examining the interactions between convection and disturbances based on datasets covering longer periods with a spatial resolution high enough to resolve it.

Acknowledgements

The authors would like to thank Drs M. Satoh, M. Sugi, T. Miyakawa, S. Nishizawa, S. Iga, and H. Miura, T. Nasuno and our colleagues for fruitful discussions. The simulation was performed using the K computer at the RIKEN Advanced Institute for Computer Science.

References

Houze RA Jr. 1994. *Cloud Dynamics*. Academic Press: San Diego, CA; 573 pp.

Kalnay E, Kanamitsu M, Kistler R, Collins W, Deaven D, Gandin L, Iredell M, Saha S. 1996. The NCEP/NCAR 40-year reanalysis project. *Bulletin of the American Meteorological Society* **77**: 437–471, doi: 10.1175/1520-0477(1996)077<0437:TNYRP>2.0.CO;2.

Kikuchi K, Wang B, Kajikawa Y. 2012. Bimodal representation of the tropical intraseasonal oscillation. *Climate Dynamics* **38**: 1989–2000, doi: 10.1007/s00382-011-1159-1.

Liebmann B, Smith CA. 1996. Description of a complete (interpolated) outgoing longwave radiation dataset. *Bulletin of the American Meteorological Society* **77**: 1275–1277.

Louis JF. 1979. A parametric model of vertical eddy fluxes in the atmosphere. *Boundary-Layer Meteorology* **17**: 187–202, doi: 10.1007/BF00117978.

Madden RA, Julian PR. 1994. Observations of the 40-50-day tropical oscillation-a review. *Monthly Weather Review* **122**: 814–837, doi: 10.1175/1520-0493(1994)122<0814:OOTDTO>2.0.CO;2.

Miyamoto Y, Kajikawa Y, Yoshida R, Yamaura T, Yashiro H, Tomita H. 2013. Deep moist atmospheric convection in a subkilometer global simulation. *Geophysical Research Letters* **40**: 4922–4926, doi: 10.1002/grl.50944.

Miyamoto Y, Satoh M, Tomita H, Oouchi K, Yamada Y, Kodama C, Kinter J III. 2014. Gradient wind balance in tropical cyclones in high–grid spacing–global experiments. *Monthly Weather Review*, **142**: 1908–1926, doi: 10.1175/MWR-D-13-00115.1.

Nakanishi M, Niino H. 2004. An improved Mellor–Yamada Level-3 Model with condensation physics: its design and verification. *Boundary-Layer Meteorology* **112**: 1–31, doi: 10.1023/B:BOUN.0000020164.04146.98.

Noda AT, Oouchi K, Satoh M, Tomita H, Iga S. 2010. Importance of the subgrid-scale turbulent moist process: Cloud distribution in global cloud-resolving simulations. *Atmospheric Research* **86**: 208–217, doi: 10.1016/j.atmosres.2009.05.007.

Renard RJ, Clarke LC. 1965. Experiments in numerical objective frontal analysis 1. *Monthly Weather Review* **93**: 547–556, doi: 10.1175/1520-0493(1965)093<0547:EINOFA>2.3.CO;2.

Rossow WB, Schiffer RA. 1999. Advances in understanding clouds from ISCCP. *Bulletin of the American Meteorological Society* **80**: 2261–2287, doi: 10.1175/1520-0477(1999)080<2261:AIUCFI>2.0.CO;2.

Satoh M, Matsuno T, Tomita H, Miura H, Nasuno T, Iga S. 2008. Nonhydrostatic icosahedral atmospheric model (NICAM) for global cloud resolving simulations. *Journal of Computational Physics* **227**: 3486–3514, doi: 10.1016/j.jcp.2007.02.006.

Sekiguchi M, Nakajima T. 2009. The improvement of the absorption process using a computational optimization in an atmospheric general circulation model, vol. 89, International Radiation Symposium, 1100.

Smith RK. 2000. The role of cumulus convection in hurricanes and its representation in hurricane models. *Reviews of Geophysics* **38**: 465–489.

Tomita H. 2008. New microphysical schemes with five and six categories by diagnostic generation of cloud ice. *Journal of the Meteorological Society of Japan Ser II* **86A**: 121–142, doi: 10.2151/jmsj.86A.121.

Tomita H, Satoh M. 2004. A new dynamical framework of nonhydrostatic global model using the icosahedral grid. *Fluid Dynamics Research* **34**: 357–400, doi: 10.1016/j.fluiddyn.2004.03.003.

